Acta Materialia 135 (2017) 226–232

Contents lists available at ScienceDirect

Acta Materialia

journal homepage: www.elsevier.com/locate/actamat

Full length article

Two modes of grain boundary pinning by coherent precipitates

Nan Wang [a, b, *], Yanzhou Ji [b], Yongbiao Wang [b], Youhai Wen [c], Long-Qing Chen [b]

[a] Physics Department, McGill University, Montreal, Quebec H3A2T8, Canada
[b] Department of Materials Science and Engineering, Pennsylvania State University, University Park, PA 16802, USA
[c] National Energy Technology Laboratory, Albany, OR 97321, USA

ARTICLE INFO

Article history:
Received 24 December 2016
Received in revised form
13 June 2017
Accepted 14 June 2017
Available online 18 June 2017

Keywords:
Grain growth
Grain boundary
Coherent precipitate
Particle pinning
Phase-field-crystal model

ABSTRACT

We propose a two-mechanism theory to estimate the pinning effect of coherent precipitates on grain-boundary (GB) migration in grain growth, taking into account the important effect of elastic misfit strain at the coherent interface. Depending on the relative importance of the elastic and the GB contributions to the total free energy, Zener type stabilization or a novel elastic energy induced stabilization may occur. It is found that the pinning is most effective in the crossover region between these two mechanisms. A phase-field-crystal model is used to numerically validate the theory. Relevant experiments and potential impacts on alloy design are also discussed.

1. Introduction

Second-phase precipitates formed in alloy microstructure strengthen materials by blocking dislocation motion or stopping grain growth at elevated temperature and therefore limiting the propagation of plastic deformation [1–3]. There have been extensive studies on the interactions between precipitates and GBs in order to understand their inhibiting effect on grain growth and improve materials strength [4–8]. Precipitates can generally be separated into two types: coherent and incoherent. For coherent precipitates within a given grain, the lattice planes across the interfaces between the precipitates and grain matrix are continuous, and the lattice parameter differences between the precipitates and matrix are accommodated by elastic strains. Therefore, coherent interfaces have relatively small interfacial energy, but they generate strain energy. For incoherent precipitates, the lattice planes for the precipitates and matrix grain terminate at their interfaces. Incoherent interfaces generally possess higher interfacial energy while the shear strain energy is relaxed.

Although coherent precipitates have long been believed to be effective pinning units for GB migration, the role of the elastic strain in GB pinning has not yet been fully understood. Existing investigations have been largely focused on the interactions between incoherent precipitates and GBs in limiting grain growth [2,5,6,9] described by Zener's theory which takes into account only the interfacial energy contributions in pinning [10,11]. Pinning force from coherent particles has been calculated based on Zener's theory. It is shown that, by only considering interfacial energies, coherent particles are more effective in pinning GB migration. The classic continuum elasticity theory works well for describing the dislocation-coherent particle interactions. However, it is a challenge to generalize it to describing the GB-coherent particle interactions due to the fact that a segment of the coherent particle-matrix interface loses its coherency when a GB replaces it during the migration, partially relaxing the elastic energy. The change of interface coherency in turn modifies the stress distribution along the remaining coherent part of the interface and affects the GB migration near the particle.

To reveal the interaction mechanisms between a GB and a coherent interface during the GB migration generally requires a sophisticated computational approach at the continuum level. To avoid the complication introduced by the moving GB and the change of interface property, we propose a qualitative theory to estimate the effect of misfit generated elastic energy on the GB migration based on energy competition criterion using a simplified interface geometry. The phase-field-crystal model (PFC) which naturally captures the effect of elasticity and the change of

* Corresponding author. Physics Department, McGill University, Montreal, Quebec H3A2T8, Canada.
E-mail address: n11wang@yahoo.com (N. Wang).

http://dx.doi.org/10.1016/j.actamat.2017.06.031
1359-6454/

interface coherency, and operates at grain growth related long time scale, is then used to examine the atomistic interaction mechanisms between a migrating GB and a coherent particle.

2. Theory

The particle pinning theory in grain growth, as formulated by Zener, is based on the balance of interfacial energies at the contact point [2]. When a second-phase particle intersects with a moving GB, it forms a new interface with the growing grain, replacing the original interface with the shrinking grain. The GB-particle contact point in 2-dimension (2D) or the contact line in 3-dimension (3D) becomes a triple junction (line). The line tensions from the two particle-grain interfaces and the GB need to balance each other along the tangential direction of the particle-grain interface for the configuration to be stable. Since the GB motion from the growing grain to the shrinking grain is driven by the macroscopic curvature effect (the grain size is usually much larger than the second-phase particle), stable configuration of the GB in this case is a bow-out shown in Fig. 1 [12]. For a system with large grain size, the driving force for the GB motion from the grain curvature is generally small, and the curved configuration of the GB near the particle can generate enough pinning force to stop the GB migration. At smaller grain size, the curved GB around the particle is subject to a larger driving force from increased grain curvature and may not be able to entirely pin the GB migration.

One can write this process as a minimization problem based on a free energy functional. In the simple two-grain case shown in Fig. 1, it is

$$F_0 = \sum_i l_i\gamma_i + \int \Delta\mu dv + \int f_{el} dv \tag{1}$$

where dv is volume element, γ is interfacial energy, l is interface length (in 2D), the summation subscript i covers the GB and the two particle-grain interfaces, f_{el} is the elastic energy density, $\Delta\mu = \alpha\gamma_{GB}/D$ is the chemical potential difference for atoms across the grain boundary. It is proportional to the GB energy (γ_{GB}) over the grain diameter (D) with the proportional constant α related to grain shape. The minimization of F_0 is then constrained by the line tension balance condition tangential to the particle-matrix interface. Many previous computational works on particle pinning have been using this energy minimization approach without considering the elastic energy contribution [13,14]. When there is no driving force for grain growth, the total energy F_0 with elastic contribution is then $F_0 = 2\pi R\gamma + B\pi R^2\delta^2$ where R is the 2D particle radius, δ is the particle-matrix lattice misfit, and B is a constant proportional the elastic modulus of the system. To arrive at this formula from Eq. (1), we only include a single particle-matrix interface. The elastic energy expression is based on the Eshelby's inclusion theory [15]. It has been known that the total energy F_0 can be minimized for two limiting cases. Given a constant δ, precipitates with small radius form coherently in the matrix since the added elastic contribution is smaller than the cost of switching the particle-matrix interface from low energy coherent configuration to high energy incoherent one. On the other hand, since the elastic contribution ($\sim R^2$) will eventually dominate over the interfacial energy contribution as the radius grows; large precipitates then form a high energy incoherent interface with the matrix to relax the elastic strain energy. This competing elastic strain energy and interfacial energy also explain the commonly observed phenomenon of precipitate coherency loss after swept by a GB. For a typical metal system with GB energy $\gamma \sim 1J/m^2$ lattice misfit $\delta \sim 5\%$ and elastic modulus $B \sim 100GPa$, the elastic energy $B\pi R^2\delta^2$ will surpasses the interfacial energy $2\pi R\gamma$ when the particle size is on the order of 10 nm. It also suggests that, if the elastic energy is small, precipitates would energetically prefer to form a coherent interface with the new host grain [16–18].

Similar to the steady-state energy argument discussed above, we can estimate the driving force for the grain boundary migration. To extend the Zener pinning theory which only considered interfacial energies, we also include the contribution of elastic strain energy to the pinning effect of coherent precipitates. If the elastic energy contribution is much larger than the interfacial energy, the evolution of interface configuration is then mainly driven by the minimization of $(\Delta\mu + f_{el})$. By wrapping the GB around the particle, the total elastic energy can be significantly decreased from the coherency loss at the interface while the only price paid is the increase of the total GB energy due to elongated GB length which is less significant in this limit. An interface geometry similar to the Zener pinning is then formed (Fig. 2c). It is expected that the largest elastic energy density appears near the coherent interface. Therefore, in addition to the Zener surface tension balance condition, the GB migration near the particle

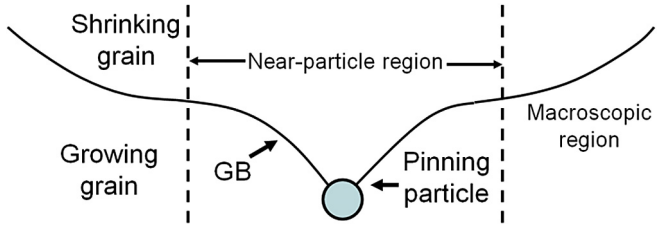

Fig. 1. A schematic showing the Zener particle pinning geometry. Far away from the pinning particle (macroscopic region), the GB has a curvature given by the grain size. Near the particle, the GB changes significantly from the shape in the macroscopic region and forms a bow-out configuration.

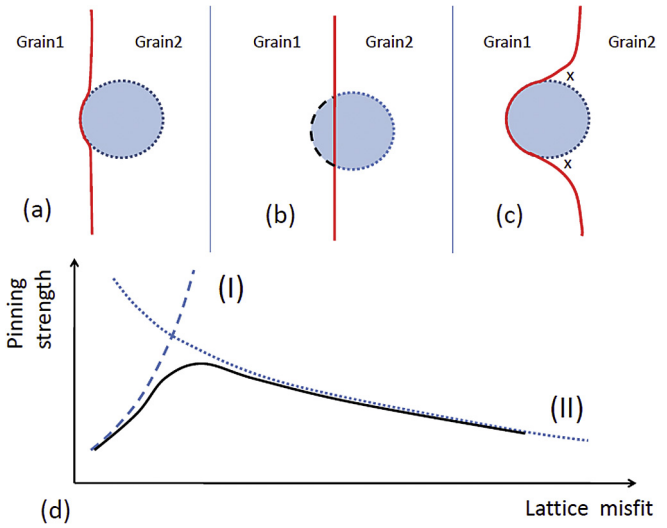

Fig. 2. Illustration of the particle-GB interaction and the pinning strength of coherent precipitates. The GB is migrating from the left to the right. Red solid line is the GB/incoherent interface. Blue dotted line is the original coherent interface the particle formed with grain 2. The small elastic energy case is shown in (a). To further migrate GB from (a), a new coherent interface with grain 1 (black dashed line) can form as shown in (b). The large elastic energy case is shown in (c) with high elastic energy density region marked by "x". A possible crossover behavior is demonstrated in (d) where the dashed line (I) is based on the small elastic energy case and the dotted line (II) is based on the large elastic energy case, the result pinning strength is shown as the solid line. (For interpretation of the references to colour in this figure legend, the reader is referred to the web version of this article.)

becomes easier with the large elastic energy density near the coherent part of the triple junction since the motion of the GB eliminates more coherent interface and reduce the associated elastic energy. From this point of view, one would expect that pinning strength is reduced by increasing elastic energy (branch II in Fig. 2d).

If the elastic energy contribution is much smaller than the interface contribution, the GB can only be elongated slightly at the early stage due to the chemical potential term and the surface tension balance condition [19,20] as shown in Fig. 2a. Since the previously explained steady-state energy argument suggests that a new coherent interface can be formed at the particle-GB interaction stage as illustrated in Fig. 2b, the Zener pinning geometry becomes invalid in this case since the GB is no longer curved around the particle. As a result, the pinning force in this case cannot come from the Zener type surface tension balance criterion with elastic correction as we argued for the large elastic energy case. An effective pinning force from the energy cost associated with the formation of the new coherent interface is proposed in the following. As shown in Fig. 2a–b, in order for the GB to move further, a coherent interface between the particle and the growing grain needs to be formed. The length of the newly formed coherent cap is proportional to the particle radius R, and the elastic energy cost is roughly the length of the cap times the misfit square $\sim R\delta^2$. Therefore, the chemical potential difference that drives the grain growth has to be larger than this elastic energy required to form the new interface in order to further migrate the GB. This new source of pinning force suggests that the pinning strength of coherent particles increases with larger elastic contribution (branch I in Fig. 2d).

Now we can combine the two sides of the story. If the elastic energy is much larger than the surface energy contribution in the system, the GB migration is promoted by further increasing elastic energy. While the pinning effect increases as the coherent precipitates introduce more elastic energy into the system only if that elastic energy is still small comparing to the interfacial energy contribution. A crossover region is then expected as the elastic contribution increases. The only elastic factor required to introduce elastic energy in the system is the particle-matrix lattice misfit since its elastic contribution to the total energy of the system will appear regardless of modulus difference. Based on the arguments above, a possible scenario is that the pinning effect of the coherent particles increases first at small misfit, reaches a plateau and further decreases with larger misfit as shown schematically in Fig. 2d.

3. Numerical model

To further validate the 2-mode mechanism we proposed above, a recently developed computational model, the phase-field-crystal method, is adapted to examine the effect of coherency strain from pinning particles on a migrating GB. Derived from the classic density functional theory (CDFT) [21], the PFC model has naturally incorporated lattice defects such as dislocations and GBs, and is capable of evolving microstructure with atomic details at long diffusion time scale. While the change of the interface structure as it switches between coherent and incoherent can be captured using most atomic level methods, the time scale of the GB migration associated with this interaction is generally beyond reach unless the grain size becomes comparable with the size of the coherent particle [22]. Instead of tracking atoms explicitly in most atomistic methods, CDFT works with an atom density field. The energy functional for single component materials in CDFT is [21,23]

$$\frac{F_{CDFT}(n)}{K_BT} = \int \{[1+n(r)]ln[1+n(r)] - n(r)\}dr - \frac{1}{2}\int dr n(r)\int C_2(r,r')n(r')dr' + high\ \ order\ \ correlations \quad (2)$$

where n is the deviation of atomic density from its average, r is spatial coordinate and $C_2(r,r')$ is the pair correlation function between r and r'. By using the density description, this method integrates out short time scale atom fluctuations and focuses on the change of statistical feature in the density field at long time scale. The PFC method is shown to be an efficient alternative to CDFT formulation [23]. While the PFC energy functional has a different form, it maps to the CDFT energy functional truncated at the pair correlation level. In this work, we choose to use the simple triangular PFC model [24] to study the particle-GB interaction.

The energy functional in the triangular PFC model is [24,25]

$$F = \int \left\{\frac{\phi}{2}\left[-\varepsilon + \left(q^2+\nabla^2\right)^2\right]\phi + \frac{\phi^4}{4} + A\phi f_{ori}\right\}dv \quad (3)$$

with volume element dv, dimensionless PFC density field $\phi = (\rho-\rho_0)/\rho_0$ where ρ is material density, ρ_0 is the reference liquid density around which the F is expended, and model parameter ε which resembles the temperature. In 2D, it favors a triangular lattice structure with lattice parameter $a = q^{-1}4\pi/\sqrt{3}$ below melting temperature ε_c. Parameter q gives the position of the first peak in the pair correlation function. By choosing model parameter ε and average density ϕ_0 corresponding to the solid phase [24], this method has been used to successfully capture many solid-state phenomena like grain growth [25], structural transitions [26] and dislocation dynamics [27]. The last term f_{ori} is a bias function that distinguishes different lattice orientations, $A = D_0/D$ is an amplitude factor related to the grain size D scaled by a reference size D_0. Together, $A\phi f_{ori}$ has the same effect as the $\Delta\mu$ term in Eq. (1), i.e. it gives the grain size dependent driving force in grain growth. Validations of this approach are shown in Fig. 3 and Fig. 4. Since the lattice misfit is the main elastic effect, one can introduce a coherent particle in the PFC functional by making q in the particle region different from the matrix. While this approach completely ignores compositional difference, it preserves the essential elastic effect a coherent particle has in the matrix. Specifically, a smooth interpolation of q^2 with $q^2 = q^2_{particle}$ inside the particle and $q^2 = 1$ in the matrix is used $q^2 = 1 + (q^2_{particle} - 1)[1 - \tanh(R^2 - R_0^2)]$ with $R^2 = (x-x_0)^2 + (y-y_0)^2$, R_0 is particle radius, and (x_0, y_0) is the coordinates of particle center. The lattice misfit δ is then related to q by $\delta = a_{particle}/a_{matrix} - 1 = 1/q_{particle} - 1$. Although, by manually introducing the spatial dependence of q, the shape and the size of the particle become independent from the particle-GB interaction, it is a common assumption used in particle pinning studies and can be deemed as a slow diffusion limit of the particle atoms. A simple energy minimization procedure based on variational principle

$$\frac{\partial\phi}{\partial t} = -\frac{\delta F}{\delta\phi} + \lambda, \quad (4)$$

is then used to evolve the density field. The total density of the system is conserved using the Lagrange multiplier $\lambda = \frac{1}{L_xL_y}\int\frac{\delta F}{\delta\phi}dv$ in 2D where the numerical domain size is given by L_x and L_y.

To drive the motion of a flat grain-boundary in this PFC model, the lattice orientation energy bias similar to the one used in the structural PFC model to study solute dragging effect in GB motion

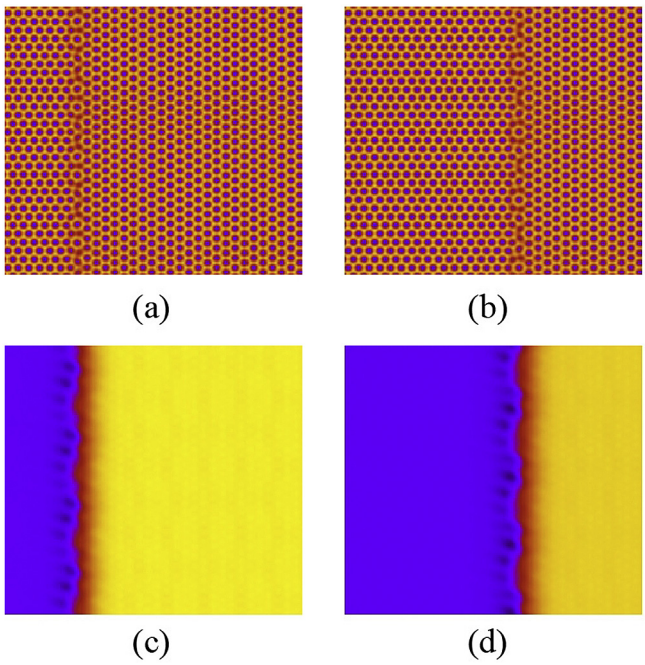

Fig. 3. Effect of the orientation tilt function in bi-crystal setting. (a) and (b) are plots of PFC density field, (c) and (d) are plots of corresponding tilt function. Dark color in (c) and (d) maps to smaller f_{ori} while light color maps to larger value. Model parameter $\overline{\phi} = 0.2$, $\varepsilon = 0.12$. (For interpretation of the references to colour in this figure legend, the reader is referred to the web version of this article.)

[28] is formulated here. To construct f_{ori} that efficiently distinguishes one local lattice orientation from another; we first calculate the convolution of density field ϕ with a wavelet function and then smooth the result with another Gaussian convolution [29]. The wavelet convolution kernel can be constructed as the product of the one-mode PFC lattice and a Gaussian envelope

$$C_1 = \frac{1}{\sigma_1\sqrt{\pi}} e^{-\frac{(x-x_0)^2+(y-y_0)^2}{2\sigma_1^2}} \left[\cos\left(\frac{\sqrt{3}}{2}\tilde{x}\right)\cos\left(\frac{1}{2}\tilde{y}\right) - \frac{1}{2}\cos(\tilde{y})\right] \quad (5)$$

where σ_1 is the profile width and the wavelet is centered at (x_0, y_0). The wavelet lattice orientation can be tuned by introducing a simple rotation $\tilde{x} = (x - x_0)\cos\theta_1 - (y - y_0)\sin\theta_1$, $\tilde{y} = (y - y_0)\cos\theta_1 + (x - x_0)\sin\theta_1$ with rotation angle θ_1. The second Gaussian smoothing kernel is

$$C_2 = \frac{1}{\sigma_2\sqrt{\pi}} e^{-\frac{(x-x_0)^2+(y-y_0)^2}{2\sigma_2^2}} \quad (6)$$

where σ_2 is the profile width. Convolutions can then be efficiently calculated using Fast Fourier Transform and convolution theorem. The orientation dependent function is then

$$f_{ori} = (\phi * C_1) * C_2, \quad (7)$$

where * is the convolution operation. Note, for the first wavelet convolution, only positive part of the result is kept. Numerically, by choosing $\sigma_1^2 = 8$ and $\sigma_2^2 = 14$, the resulted f_{ori} is smooth and yet spatially well resolved.

To demonstrate the effect of this tilt function, it is applied to a bi-crystal system with a high angle grain boundary (misorientation $\pi/6$) as shown in Fig. 3. Model parameters ε and ϕ_0 are chosen such that the system corresponds to a high temperature solid in the phase diagram in Ref. [24].

By adding this tilt term in the energy functional and aligning the wavelet convolution kernel with the right grain, the flat GB in the bi-crystal setting moves from the left to the right since such a motion eliminates the high energy orientation as shown in Fig. 3. Migration velocity of the flat GB under this energy tilt function is examined in Fig. 4.

Grain growth is typically seen as a curvature driven phenomenon where the GB migration is driven by curvature-induced chemical potential difference of atoms. The parameter $A = D_0/D$ used in the computational model controls the chemical potential difference between the two grains as shown in Fig. 3. By varying the parameter A, the driving force of grain growth due to different grain size D can be obtained. It is well known that GB migration velocity is proportional to 1/D. The linear dependence of GB migration velocity as a function of $A = D_0/D \sim 1/D$ shown in Fig. 4 demonstrates that our computational approach can reproduce this commonly accepted GB migration velocity. Since the PFC density field is periodic, the boundary motion is also affected by this periodic lattice similar to the Peierls-Nabarro barrier effect in dislocation motion. The tilt amplitude has to be large enough to initiate the GB motion. Once the motion is activated, it forms an ideal linear relation with the tilt amplitude after the small "take-off" region. One should be noted that the velocity shown in Fig. 4 is a long time averaged result. The motion becomes oscillatory in time near the low velocity end.

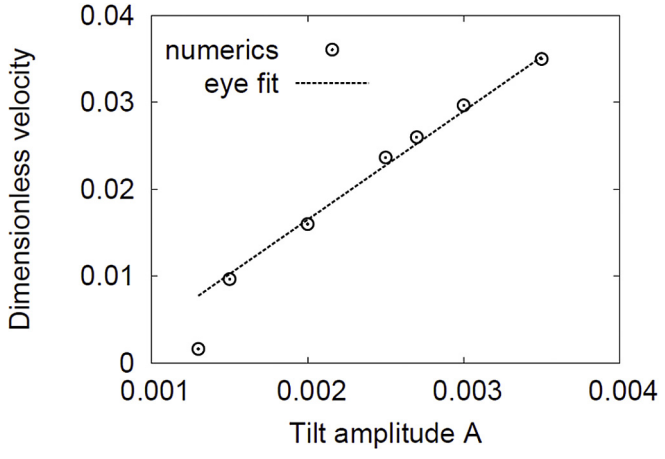

Fig. 4. Migration velocity of the flat high angle GB in Fig. 3 with different tilt amplitude A.

As a further validation of this computational approach, GB interaction with an incoherent particle is simulated. A simple bi-crystal setup with the energy bias function f_{ori} favors the left grain over the right one is used. An incoherent particle is manually put in the right grain. The classic Zener pinning behavior in which the GB follows the normal direction of the particle matrix interface is demonstrated in Fig. 5a–c.

Numerical investigation of the particle-GB interaction is focused on 2D case since it is much less computationally demanding. Although the 2D result is different from the 3D result in the classic pinning theory [2], the proposed elastic factor in pinning behavior due to the particle-matrix interface coherency is active in 2D. Also, only high-angle GB is studied in this work, since low-angle GB in 2D can be seen as a collection of dislocations. A coherent particle is introduced in the right grain by changing the lattice parameter. The particle-GB interaction is tracked using Eq. (4). The elastic effect from lattice coherency is studied by checking the smallest grain size at which the coherent particle can stabilize as a function of the

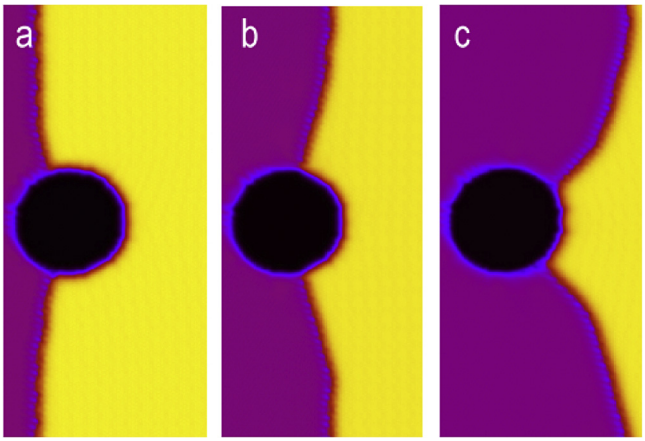

Fig. 5. GB interaction with an incoherent particle simulated using the PFC approach. Figures (a)–(c) are time sequence. Two grains are colored based on their corresponding chemical potential. Atomic level details are smoothed out. The purple grain is growing and the yellow one is shrinking. The incoherent particle is shown in black. (For interpretation of the references to colour in this figure legend, the reader is referred to the web version of this article.)

lattice misfit. Pinning effect of the particle is measured by the maximum grain-boundary migration driving force (A~1/D) it can block.

4. Results and discussions

The numerical results in Fig. 6 exhibit a crossover behavior as we expected in Fig. 2. With small misfit, the blocking effect of the coherent particles against GB migration increases with elastic misfit. With large lattice misfit, the blocking strength decreases with further increasing elastic effect. The simulation results also demonstrate that there are two different modes of the pinning effect depending on the final coherency state of the particle-matrix interface as shown in Figs. 6 and 7. In region I, a new coherent particle-matrix interface is formed with the growing grain as shown in Fig. 7a–c, and the pinning effect of coherent particles increases with elastic misfit. In region II, the particle-matrix interface becomes incoherent (Fig. 7d–f) and the pinning effect decreases with lattice misfit. To better demonstrate the formation of coherent and incoherent interfaces, atomic configuration of the interfaces of Fig. 7b and e are shown in Fig. 7g and h. Essential

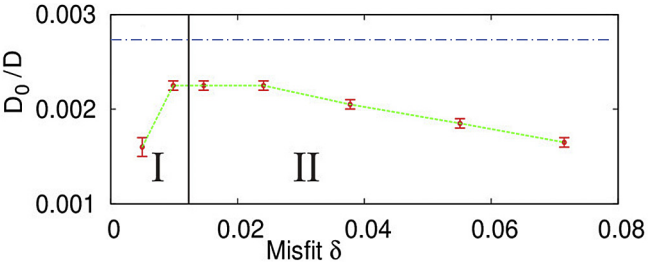

Fig. 6. PFC numerical results for the pinning effect of coherent particles against GB migration with different lattice misfit. Two regions I and II are separated based on the final state of the particle-matrix interface. In region I, a coherent interface is formed. In region II, an incoherent interface is formed. Error bars mark the nearest simulation sample. The dotted line is a simple connection of simulation points. As a comparison, pinning effect from an incoherent particle of the same size is shown as the dashed straight line above the dotted line. Particle size $R = 100$ or $R/a = 14$. Average density $\overline{\phi} = 0.2$, $\varepsilon = 0.12$. GB misorientation angle is $\pi/6$. Simulation box size $L/R = 8$. Error bars mark the nearest simulation sample points.

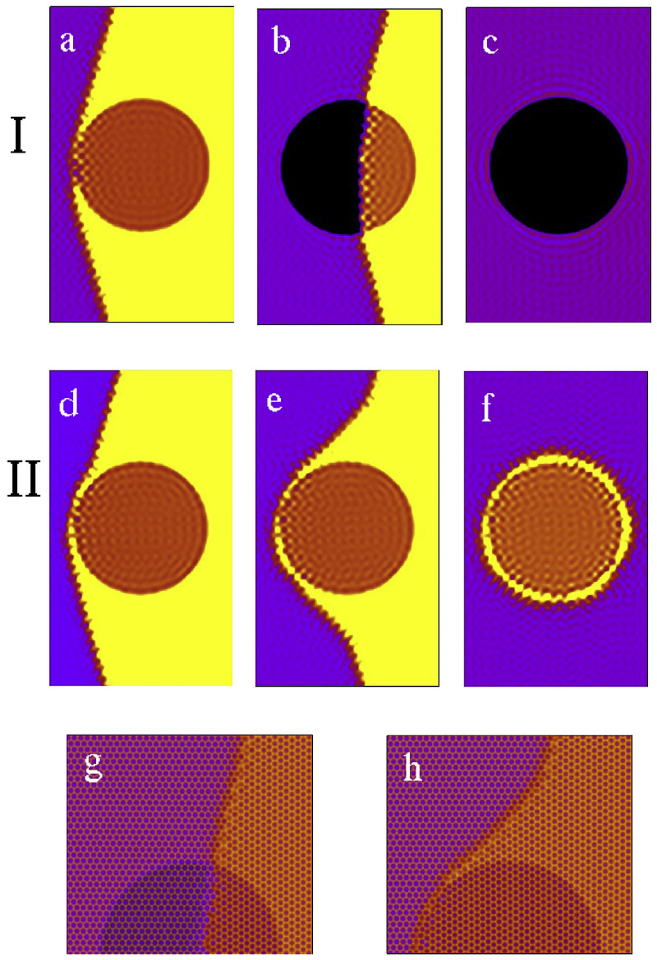

Fig. 7. Two migration mechanisms of the GB near the coherent particle. Figures (a)–(f) are colored based on both the lattice orientation and the lattice parameter with smoothed out atomic details. Purple and yellow are used for the lattice orientation of the growing grain and the shrinking grain respectively. The particle region is shown in darker color due to its lattice parameter difference with the matrix (It is colored as dark yellow when it has the same lattice orientation with the yellow grain. When it switches its orientation to follow the purple grain, the color is shown as black.). Atomic density field for the upper half of (b) and (e) are shown in (g) and (h). Each small dark dot corresponds to an atom position. To better visualize the particle and the grains, the density field is superimposed with the corresponding colored figure. (For interpretation of the references to colour in this figure legend, the reader is referred to the web version of this article.)

features of our theory in Fig. 2 are qualitatively validated.

Pinning effect from an incoherent particle of the same size is also included in Fig. 6. It has been known from Zener's theory that coherent particles usually have stronger pinning effect comparing with incoherent particles. However, our result in Fig. 6 suggests that an incoherent particle can have stronger pinning effect than a coherent one. This seemingly inconsistency can be understood by considering the elastic effect. In the theory section, we summarized that the interfacial energy induced pinning mode (Zener's theory, or Fig. 2c and branch II in Fig. 2d) is active when the elastic energy required to activate the other pinning mode (Fig. 2a and branch I in Fig. 2d) is much larger than the cost of curving the GB around the particle. Since the Zener's theory does not consider elastic energy, the less costly elastic pinning mode (branch I in Fig. 2d) at small misfit is then replaced by the interfacial energy induced pinning mode shown in the branch II of Fig. 2d. Based on the argument following Fig. 2c, the interfacial energy induced pinning mode is most effective when there is no elastic energy involved. Therefore,

the stronger coherent particle pinning effect seen in the Zener's theory is consistent with our theory, and it can be seen as a special case of the branch II pinning mode with zero elastic effect.

The coherent particles are well known to contribute considerably for the strengthening effect in various alloy systems, for example, L12-ordered particles in fcc matrices, such as spherical or cuboidal γ'-Ni_3Al in Ni-based alloys [30,31] and Al_3Sc in Al-Sc-based alloys [32,33]. Although, part of the contribution comes from the precipitate strengthening through the interaction with dislocations, they also act as pinning points for GB migrations. However, the pinning effect of these particles, especially the correlation between the stable grain size and the particle elastic properties, is not yet well understood. The difficulty lies in the complexity of the system. Firstly, due to the multi-component nature of the alloy system, the incoherent or inert particles can also appear in the system to provide the Zener pinning, which will add to the difficulty to extract the pinning effect purely by the coherent particles. Secondly, the particle elastic property is highly dependent on the alloying components and compositions, as well as heat treatment temperatures, and is therefore difficult to estimate experimentally or empirically.

To our knowledge, there is no explicit theory that provides a connection between the particle elastic properties and the pinning effect. The theory and numerical results we reported above between the lattice misfit and the pinning strength may provide further information in alloy design beyond current thermodynamic schemes since the precipitate lattice parameter changes with alloy concentration and components. Currently, a few systems have data available to obtain the relationship between the stable grain size and the particle-matrix lattice misfit. One example is coherent γ'-Ni_3Al particles in an IN100-type superalloy [30]. It has been reported that the pinning effect of γ' particles is dominant below the solvus temperature of γ' phase, where the amount of γ' particles win over inert particles [30]. Moreover, the lattice parameters of γ and γ' phases as a function of alloy compositions and temperatures have been established [34] for estimation of the particle-matrix lattice misfit. Therefore, the correlation between the stable grain size and the particle-matrix lattice misfit can be established for sub-solvus temperatures for this system, showing the decrease of limiting grain size with the increase of the particle-matrix lattice misfit which is consistent with our theory for region I. However, due to the limited number of investigations in this study, the decrease of the pinning effect with further increase of lattice misfit is not captured. Most recently, experimental measurement of the lattice misfit in an Al-Mg-Si alloy is obtained using scanning transmission electron microscopy [35]. It confirms the misfit result of a previous computational study using density functional theory [36].

As shown in Fig. 6, only the pinning mode induced by elastic energy at small misfit is enhanced by increasing elastic effect, while the interfacial energy induced pinning mode becomes less efficient with increasing elastic energy. Although the crossover behavior shown in Fig. 6 is a result of the two competing modes, an estimation of relevant pinning mode that one may expect in experiments could be useful. A very rough estimation can be made based in the relative importance of elastic and interfacial energy in the system without considering GB migration. With typical material parameters $\gamma \sim 1J/m^2$ and elastic modulus $B \sim 100GPa$, a coherent particle of 30 nm size with 10% lattice misfit would likely to exert its pinning effect through the interfacial energy induced pinning mode (region II) since the elastic energy $B\pi R^2\delta^2$ is on the order $10^{-6}J$ and is much larger than the interfacial contribution $2\pi R\gamma$ which is on the order of $10^{-7}J$. For the same size particle with a lattice constant similar to the matrix (1% misfit), it is likely to show its pinning effect through the elastic energy induced mode (region I) since the interfacial energy involved ($10^{-7}J$) is much larger than the elastic energy there ($10^{-8}J$). Particle shape is another known factor that may significantly modify the pinning effect. Previous works on the particle shape effect are mostly based on Zener's theory. Since the particle shape can strongly affect the distribution of local elastic energy near the particle, one may expect a similar shape dependence in the two-mode theory proposed in this work. Many realistic second phase particles have not only a lattice misfit but also a compositional or a lattice structure difference from the matrix. To highlight the elastic effect, our current model does not consider these additional effects. Numerical investigation on the effect of particle shape, compositional difference and lattice structure difference can be carried in the future since relevant PFC models are available.

In summary, the effect of misfit generated elastic energy in the GB-coherent particle interaction is estimated and numerically validated. An elastic energy induced GB pinning mechanism is identified. Depending on the relative importance of the elastic and the interfacial energy, coherent particles go through two different pinning scenarios. The largest pinning effect is achieved in the crossover region of the two scenarios. The reported relation between the grain size and the precipitates lattice misfit may provide further guidance to improve particle pinning effect and alloy design.

Acknowledgments

NW is partially supported by funding from The National Science and Engineering Research Council of Canada. LQC is supported by the Hamer Professorship.

References

[1] E. Nembach, Particle Strengthening of Metals and Alloys, John Wiley & Sons, 1997.
[2] E. Nes, N. Ryum, O. Hunderi, On the Zener drag, Acta Metall. 33 (1985) 11.
[3] T. Gladman, Mater. Sci. Tech. Precip. Hardening Met. 15 (1999) 30.
[4] C.S. Smith, Grains, phases, and interphases: an interpretation of microstructure, Trans. Metall. Soc. A.I.M.E. 175 (1948) 15.
[5] J.E. Burke, D. Turnbull, Recrystallization and grain growth, Prog. Metal Phys. 3 (1952) 220.
[6] M. Hillert, On the theory of normal and abnormal grain growth, Acta Metall. 13 (1965) 227.
[7] P.A. Manohar, M. Ferry, T. Chandra, Five decades of the zener equation, ISIJ Inter 38 (1998) 913.
[8] E. Nembach, Synergetic effects in the superposition of strengthening mechanisms, Acta Metall. Mater. 40 (1992) 3325.
[9] F.J. Humphreys, M. Hatherly, Recrystallization and Related Annealing Phenomena, Elsevier, 2004.
[10] M.F. Ashby, J. Harper, J. Lewis, The interaction of crystal boundaries with second-phase particles, Trans. Metall. Soc. A.I.M.E. 245 (1969) 413.
[11] W. Li, E. Easterling, The influence of particle shape on Zener drag, Acta Metall. 38 (1990) 1045.
[12] P. Hellman, M. Hillert, Effect of second-phase particles on grain growth, Scand. J. Metall. 4 (1975) 211.
[13] N. Moelans, B. Blanpain, P. Wollants, Phase field simulations of grain growth in two-dimensional systems containing finely dispersed second-phase particles, Acta Mater. 54 (2006) 1175.
[14] C. Schwarze, R.D. Kamachali, I. Steinbach, Phase-field study of zener drag and pinning of cylindrical particles in polycrystalline materials, Acta Mater. 106 (2016) 59.
[15] J.D. Eshelby, The determination of the elastic field of an ellipsoidal inclusion, and related problems, Proc. Roy. Soc. Lond. Ser. A 241 (1957) 376.
[16] A. Porter, B. Ralph, The recrystallization of nickel-base superalloys, J. Mater. Sci. 16 (1981) 707.
[17] V. Randle, B. Ralph, Interactions of grain boundaries with coherent precipitates during grain growth, Acta Metall. 34 (1986) 891.
[18] M.J. Jones, F.J. Humphreys, Interaction of recrystallization and precipitation: the effect of Al3Sc on the recrystallization behaviour of deformed aluminium, Acta Matar. 51 (2003) 2149.
[19] N. Wang, Y. Wen, L.Q. Chen, Pinning force from multiple second-phase particles in grain growth, Comp. Mater. Sci. 93 (2014) 81.
[20] N. Wang, Y. Wen, L.Q. Chen, Pinning force of grain boundary migration by a

coherent particle, Philo. Mag. Lett. 94 (2014) 794.
[21] T.V. Rarnakrishnan, M. Yussouff, First-principles order-parameter theory of freezing, Phys. Rev. B 19 (1979) 2775.
[22] K.G.F. Janssens, D. Olmsted, E.A. Holm, S.M. Foiles, S.J. Plimpton, P.M. Derlet, Computing the mobility of grain boundaries, Nat. Mater. 5 (2006) 124.
[23] K.R. Elder, N. Provatas, J. Berry, P. Stefanovic, M. Grant, Phase-field crystal modeling and classical density functional theory of freezing, Phys. Rev. B 75 (2007) 064107.
[24] K.R. Elder, M. Grant, Modeling elastic and plastic deformations in nonequilibrium processing using phase field crystals, Phys. Rev. E 70 (2004) 051605.
[25] K.A. Wu, P.W. Voorhees, Phase field crystal simulations of nanocrystalline grain growth in two dimensions, Acta Mater. 60 (2012) 407.
[26] M. Greenwood, N. Provatas, J. Rottler, Free energy functionals for efficient phase field crystal modeling of structural phase transformations, Phys. Rev. Lett. 105 (2010) 045702.
[27] J. Berry, N. Provatas, J. Rottler, C.W. Sinclair, Phase field crystal modeling as a unified atomistic approach to defect dynamics, Phys. Rev. B 89 (2014) 214117.
[28] M. Greenwood, C. Sinclair, M. Militzer, Phase field crystal model of solute drag, Acta. Mater. 60 (2012) 5752.
[29] H.M. Singer, I. Singer, Analysis and visualization of multiply oriented lattice structures by a two-dimensional continuous wavelet transform, Phys. Rev. E 74 (2006) 031103.
[30] K. Song, M. Aindow, Grain growth and particle pinning in a model Ni-based superalloy, Mater. Sci. Eng. A 479 (2008) 365.
[31] D.M. Collins, B.D. Conduit, H.J. Stone, M.C. Hardy, G.J. Conduit, R.J. Mitchell, Grain growth behaviour during near-γ′solvus thermal exposures in a polycrystalline nickel-base superalloy, Acta Mater. 61 (2013) 3378.
[32] N.E. Hamilton, M. Ferry, Grain growth in a nanocrystalline Al-Sc alloy, Mater. Trans. 45 (2004) 2264.
[33] M. Ferry, N.E. Hamilton, F.J. Humphreys, Continuous and discontinuous grain coarsening in a fine-grained particle-containing Al–Sc alloy, Acta Mater. 53 (2005) 1097.
[34] T. Wang, L.-Q. Chen, Z.-K. Liu, Lattice parameters and local lattice distortions in fcc-Ni solutions, Metall. Mater. Trans. A 38 (2007) 562.
[35] S. Wenner, R. Holmestad, Accurately measured precipitate–matrix misfit in an Al–Mg–Si alloy by electron microscopy, Scr. Mater. 118 (2016) 5.
[36] F.J.H. Ehlers, S. Dumoulin, R. Holmestad, 3D modelling of β″ in Al–Mg–Si: towards an atomistic level ab initio based examination of a full precipitate enclosed in a host lattice, Comp. Mater. Sci. 91 (2014) 200.